Inorganica Chimica Acta 560 (2024) 121810

Contents lists available at ScienceDirect

Inorganica Chimica Acta

journal homepage: www.elsevier.com/locate/ica

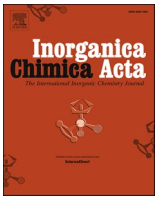

Halogen addition to NHC-gold(I) chloride complexes in the framework of the Inverted Ligand Field

Rossana Galassi [a,1,*], Nicola Sargentoni [a,2], Lorenzo Luciani [a,3], Gabriele Manca [b,4,*], Andrea Ienco [b,5]

[a] School of Science and Technology, Chemistry Division, University of Camerino, Via Madonna delle Carceri, 10, I-62032, Italy
[b] Istituto di Chimica dei Composti Organo-Metallici, CNR-ICCOM, Via Madonna del Piano 10, 50019 Sesto Fiorentino, Italy

ARTICLE INFO

Keywords:
NHC-carbenes
Gold(I)/gold(III)
Halogen addition
Inverted Ligand Field

ABSTRACT

The conversion of LAuX to $LAuX_3$, where L is a neutral ligand such as a phosphane or a carbene and X = Cl, Br or I, can be performed by halogen addition reactions in mild conditions. The formation of complexes with mixed halides, such as $LAuY_2X$, also evoking the possibility of geometrical isomerization, is less investigated. In this work the iodine and bromine addition reactions, under mild conditions, to a symmetrically disubstituted carbene 1,3-dimethyl-imidazolyl-2-yl-gold(I)chloride were considered. The molecular structures highlight the formation of the trans $LAuI_2Cl$ in the case of iodine addition and a mixture of the geometrical isomers for bromine. DFT analysis points out a stepwise addition of halogen atom to the linear gold(I) complex without a net change in metal electronic population, suggesting the occurrence of the Inverted Ligand Field.

1. Introduction

Oxidative additions as well as reductive eliminations involving transition metal complexes are ubiquitous in catalysis [1], in medicinal chemistry [2] and material science [3]. According to the traditional models, oxidative addition of a substrate to a transition metal center occurs with the increase of metal coordination and oxidation number [4]. Different mechanisms of oxidative addition can be observed highly dependent on both the metal complex and the substrate [5–7]. For years, the gold chemistry has been limited to substitution reactions or to unsaturated C—C bond activations, mainly due to a somehow gold recalcitrance to undergo oxidative addition or reductive elimination [8], on the contrary of what observed for the d^8 congeners, for example Pd(II) square planar complexes [9]. For its quite inertness, over the centuries gold has been considered as the substance closer to the perfection and many alchemical efforts have been addressed toward the transformation of more common metals in gold [10]. In this regards, *aqua regia* was considered as the universal solvent, which, through an alchemical reaction, may generate the Philospher's stone. A very beautiful representation of the central role of gold in alchemy is the metal dissolution in *aqua regia* (the universal solvent) depicted as a green lion biting a bleeding red sun (the gold) [11]. Gold recalcitrance toward the oxidation is argued within the "redox gold problem" in view of the very high oxidation potential (1.41 V) for Au(III)/Au(I) redox couple, that becomes accessible for linear LAuX systems, where L = phosphane or carbenes, and X = halides [12–14]. Square planar gold complexes could be prepared by addition reactions between linear gold(I) precursors featuring pincer CNC ligands [15], and halogens [12,16–18], or alkyl or aryl halides [19], for examples. Interestingly, the opposite process of the "reductive elimination" has been already confirmed to be particularly energy demanding with respect to the d^8 congeners [20]. In the case of the moisture stable square planar $(Ph_3P)Au(CF_3)(aryl)(I)$, the reductive elimination of C_{aryl}-CF_3 has been proposed to evolve through a tricoordinate intermediate after the removal of a ligand promoted by

* Corresponding authors at: School of Science and Technology, Chemistry Division, University of Camerino, c/o ChIP Via Madonna delle Carceri 10, I-62032 Camerino, Italy (R. Galassi).
E-mail addresses: rossana.galassi@unicam.it (R. Galassi), gabriele.manca@iccom.cnr.it (G. Manca).
[1] ORCID: 0000-0002-8025-9615
[2] ORCID: 0009-0009-2735-3440
[3] ORCID: 0000-0002-9000-7454
[4] ORCID: 0000-0003-2068-1731
[5] ORCID: 0000-0002-2586-4943

https://doi.org/10.1016/j.ica.2023.121810
Received 4 July 2023; Received in revised form 4 September 2023; Accepted 12 October 2023
Available online 13 October 2023

high temperature (122 °C), photolytic processes or silver salts adding [21]. Square planar NHC-Au(III) centers, where NHC are heterocyclic carbene ligands, can be prepared by addition of halogens [22,23] or sources of halogens [24–26] to linear NHC-AuX compounds and, so far, the outcomes are strongly case-sensitive. The choice of the oxidizing agent to prepare NHC-AuX_3 derivatives (X = Cl, Br) depends on steric constraints of substituents and/or on the reactivity toward the imidazole of the NHC ligand [27]. As an example, chlorine gas or *aqua regia* might be suitable oxidants but they may attain undesired oxidative reactions at the ligands [28]. The choice of the experimental conditions, as well as of the oxidant, discriminates the results; for instance the full oxidation in mild condition of the carbene compound {N-[(phenylseleno)-methylene)]-N′-methylimidazolyl}gold chloride was achieved with iodine (I_2) in a yield of 98 %, whereas the reaction with bromine (Br_2) led only to decomposition [29]. Noteworthy, most of the reactions of bromine with NHC-AuCl systems afford the substitution of the chloride and the total bromination of the gold center [18]. Generally, the products of these reactions are isolated as crystalline solids of the type NHC-AuX_3 where X = Cl, Br [23,30]. Additionally, depending on the nature of both the starting NHC-AuX compounds and the added halogen, the formation of mixed halide NHC-AuY_2X compounds was observed too [31–33].

Nevertheless, the widespread of halogen oxidative addition to gold (I) in the literature, the lack of some expected results, the easiness of the reversible conversion from LAuX to $LAuX_3$ or the presence of geometrical isomerism in the mixed halides Au(III) is still without explanations. Herein, the addition of halogens to linear NHC-AuCl compound was carried out choosing as reference reactions the addition of molecular iodine or bromine to linear gold(I) chlorido complexes bearing a symmetric *N*-Heterocyclic Carbene (NHC) ligand, the 1,3-dimethylimidazolyl [17]. The isolated products have been X-ray solved and the crystallographic structures are described in detail. The electronic structure of the obtained complexes has been largely reconsidered and explained in terms of the ILF with gold maintaining its starting d^{10} electronic count also in the final square planar complexes.

2. Experimental section

2.1. Syntheses

Materials have been purchased by Merck and used without any further purification. Solvents were freshly distilled before use. The synthesis of 1,3-dimethylimidazolium chloride and of 1,3-dimethylimidazolyl-2yl-gold(I) chloride (**1**) were performed following methods previously reported in literature [34–36].

2.2. Characterizations

Elemental analyses (C, H, N, S) were performed in-house with a Fisons Instruments 1108 CHNS-O Elemental Analyser. Melting points were taken on an SMP3 Stuart Scientific Instrument. IR spectra were recorded from 4000 to 600 cm^{-1} with a Perkin-Elmer SPECTRUM ONE System FT-IR instrument. IR annotations used: br = broad, m = medium, s = strong, sh = shoulder, *vs* = very strong, w = weak and vw = very weak. ^1H and ^{13}C NMR spectra were recorded on an Oxford-400 Varian spectrometer (400.4 MHz for ^1H and 100 MHz for ^{13}C). Chemical shifts, in ppm, for ^1H and ^{13}C NMR spectra are relative to internal Me_4Si. NMR annotations used: br = broad, d = doublet, dd = double doublet, t = triplet, m = multiplet, s = singlet. UV–Vis spectra were acquired using the Shimadzu UV-2700i spectrophotometer, equipped with the Shimadzu CPS-100 Peltier, at 298 K.

2.3. Synthesis of trans-(1,3-dimethylimidazolyl-2yl)-AuI_2Cl (**2**)

1,3-dimethylimidazolyl-2yl-gold(I)chloride (100 mg, 0.30 mmol) was dissolved in 20 mL of acetonitrile, under nitrogen atmosphere, and then solid iodine (114.21 mg, 0.45 mmol) was added. The reaction was stirred for 2 h under nitrogen atmosphere. After 2 h, the red solution was evaporated to dryness under reduced pressure, and the resulting reddish solid was washed with *n*-hexane (2 × 10 mL) and dried under vacuum. The microcrystalline powder is sparingly soluble in most organic solvents. Dark red crystals were obtained in two days by dissolving in warm THF and by adding a few drops of diethyl ether. M. p.: 211–214 °C. Yield 85 %.

^1H NMR (CD_3CN,δ): 7.38 (s, 2H); 3.75 (s. 3H).

MIR (cm^{-1}): 3169(w), 3137(w), 2346(w), 2315(w), 1675(w), 1575 (w), 1485(m), 1431 (w), 1398(m), 1335(w), 1228(m-s), 1149(m), 1083 (m), 1019(w), 735(s), 660(s).

FIR (cm^{-1}): 660(m-s), 499(w), 477(w), 464(w), 429(w), 351(m), 313 (m-s), 277(w), 269(w), 253(w), 243(w), 224(m), 209(w), 199(m), 177 (m), 168(w), 153(w), 152(s), 149(s), 142(m), 130(m).

Elemental analysis for $C_5H_8N_2AuI_2Cl$ calcd %: C 10.31; H 1.38; N 4.81; found %: C 10.55, H 1.39, N 4.99.

2.4. Synthesis of **3**, as $\mathbf{3}_{cis}$, 17 % and $\mathbf{3}_{trans}$, 83 %

In a round-bottom flask 1,3-dimethylimidazolyl-2yl-gold(I)chloride (99.1 mg, 0.30 mmol) was dissolved in 15 mL of acetonitrile and then, liquid bromine (72.7 mg, 23 μL, 0.45 mmol) was added. The reaction was stirred for 2 h at room temperature under nitrogen atmosphere. After 2 h, the red solution was evaporated under reduced pressure, and the resulting orange solid was washed with *n*-hexane (2 × 10 mL) and dried under vacuum. The microcrystalline powder was crystallized in acetonitrile/Et_2O; yellow-orange crystals were obtained by slow evaporation of the solvents at 5 °C. M. p.: 235–238 °C. Yield 82 %.

^1H NMR (CD_3CN,δ): 7.37 (s, br, $\mathbf{3}_{trans}$); 3.76 (s, br, $\mathbf{3}_{cis}$); 7.35 (s, br, $\mathbf{3}_{cis}$), 3.85 (s, br, $\mathbf{3}_{trans}$), (s, br, $\mathbf{3}_{cis}$).

MIR (cm^{-1}): 3170 (w), 3142 (w), 2950(w), 1689(w), 1593(w), 1574 (w), 1491(m), 1456(w), 1434(m), 1398(m), 1330(w), 1228(m-s), 1152 (w), 1086(w), 746(s), 736(s), 664(s).

FIR (cm^{-1}): 662(m-s), 611(w), 567(w), 499(w), 465(w), 455(w), 415 (w), 353(m), 342(w), 323(s), 283(m), 276(m), 246(s), 299(m), 210(w), 196(w), 185(w), 173(w), 166(w), 155(w), 148(s), 127(w), 108(s).

Elemental analysis for $C_5H_8N_2AuBr_2Cl$, calcd %: C 12.30; H 1.65; N 5.74; found %: C 12.38; H 1.62; N 5.55.

2.5. Single-Crystal X-ray diffraction (SCXRD)

Single-crystal X-ray diffraction data were collected at 100 K controlled by an Oxford Cryostream using Mo-Kα radiation (λ = 0.71073 Å) on a Bruker Apex-II diffractometer equipped with a CCD detector, controlled by APEX2 software [37]. Crystallographic data and refinement parameters are reported in Table 1. Data integration and reduction were performed using Bruker SAINT software [38]. Absorption correction was performed with the program SADABS-2016/2 [39]. The crystal structures were solved using the SIR-2004 package [40] and refined by full-matrix least squares against F^2 using all data (SHELXL-2018/3) [41]. All the non-hydrogen atoms were refined with anisotropic displacement parameters. In both cases, the asymmetric unit consists of only half of the molecule, being the gold atom, the carbon atom and the halogen atom in trans to the carbene on a 2-fold axis. For **2**, the halogen atom in trans and in cis to carbene was assigned without doubts as a chlorine and iodine species, respectively. For **3**, the solution software assigned both the trans and cis position as bromide atom. During the refinement, a close inspection of the electronic difference map pointed out the presence of a lighter element such a chlorine atom, suggesting the contemporary presence of both $\mathbf{3}_{cis}$, and $\mathbf{3}_{trans}$ isomers as it was already found for a similar mixed square planar complex [42]. The approach used is well described in a recent article by S. Parkin and *al.* [43]. The gold halogen distances were restrained to the averaged values found from a statistical analysis in the CSD database [44] and the anisotropic thermal parameters for the couples Cl1, Br1 and Cl2, Br2 have been constraint to the same values. Only the presence of the

Table 1
Crystal data for the gold square planar complexes **2** and **3**.

	2	3
Empirical formula	C5 H8 Au Cl I2 N2	C5 H8 Au Br2 Cl N2
Formula weight	582.35	488.37
Temperature	100(2) K	100(2) K
Wavelength	0.71073 Å	0.71073 Å
Crystal system	Orthorhombic	Orthorhombic
Space group	*Pbcn*	*Pbcn*
Unit cell dimensions	a = 7.5167(3) Å b = 14.9477(6) Å c = 9.5872(4) Å	a = 7.5519(2) Å b = 14.6127(3) Å c = 8.9432(5) Å
Volume	1077.19(8) Å3	986.91(6) Å3
Z	4	4
Density (calculated)	3.591 Mg/m3	3.287 Mg/m3
Absorption coefficient	19.584 mm-1	23.216 mm-1
F(000)	1016	872
Crystal size	0.09 × 0.08 × 0.07 mm3	0.08 × 0.04 × 0.03 mm3
Theta range for data collection	2.725 to 36.317°.	2.788 to 36.496°.
Index ranges	$-12\leq h\leq 12$, $-24\leq k\leq 24$, $-15\leq l\leq 15$	$-12\leq h\leq 12$, $-24\leq k\leq 24$, $-14\leq l\leq 14$
Reflections collected	86,261	70,089
Independent reflections	2621 [R(int) = 0.0656]	2432 [R(int) = 0.1032]
Completeness to theta = 25.242°	100 %	100 %
Absorption correction	Semi-empirical from equivalents	Semi-empirical from equivalents
Max. and min. transmission	0.7487 and 0.3020	0.7472 and 0.4643
Refinement method	Full-matrix least-squares on F2	Full-matrix least-squares on F2
Data / restraints / parameters	2621 / 0 / 59	2432 / 8 / 62
Goodness-of-fit on F2	1.094	1.066
Final R indices [I > 2sigma(I)]	R1 = 0.0239, w*R2* = 0.0599	R1 = 0.031, w*R2* = 0.0679
R indices (all data)	R1 = 0.0288, w*R2* = 0.0622	R1 = 0.0556, w*R2* = 0.0805
Largest diff. peak and hole	1.812 and −2.087 e.Å-3	4.23 and −2.683 e.Å-3

$R_1 = \sum|F_o^2 - \langle F_o^2\rangle|/\sum F_o^2$.
$wR2 = \{\sum[w(F_o^2 - (1/k)F_c^2)^2\ ]/\sum w|F_o^2|^2]\}^{1/2}$.

isomers $\mathbf{3_{cis}}$ and $\mathbf{3_{trans}}$ was assumed and their calculated occupancy in the crystal is 17 % and 83 % respectively based on the relative occupancies of the Cl1/Br1 and Br2/Cl2 atomic sites. Crystal-Explorer17 was used to compute the Hirshfeld surfaces (HS) and their associated 2D fingerprint plots to further investigate the intermolecular interactions [45].

2.6. Computational details

All the obtained square planar complexes have been optimized at B97D-DFT [46] level of theory within the Gaussian 16 software [47] and validated as minima by computing vibrational frequencies. All the calculations were based on the CPCM model [48] for acetonitrile solvent, the same used in the experiments. The effective Stuttgart/Dresden core *pseudo*-potential (SDD) [49] was adopted for the gold and iodine atoms, while for all the other atoms the TZVP basis set [50] has been used. The optimization of the square planar complexes has been carried out also within ORCA 5.0.3 [51] software with the inclusion of the Zero-Order Regular Approximation (ZORA) for gold and iodine without any drastic change in the electronic structure. Cartesian coordinates as well as the energetic features of all the optimized structures are reported in Supporting Information.

3. Results and discussion

3.1. Synthesis and characterization

The NHC-AuCl compound **1** was synthesized according to the mild base route reported in the literature [35,36]. Compound **1** is rather stable in solution as confirmed by the ^{1}H NMR and the UV–visible spectra recorded upon time. The ^{1}H NMR spectrum of **1** was compared with that of the corresponding bis-carbene species ruling out the presence of this latter in freshly prepared acetonitrile solution, see Fig. 1S–3S in SI. Precursor **1** was treated with iodine or bromine in CH_3CN and the products were isolated as crystals and characterized by elemental analysis, IR and UV–visible, ^{1}H and ^{13}C NMR spectroscopies and by X-ray diffraction methods. Acetonitrile was chosen as solvent for solubility issues and spectroscopic characterizations of bromine and iodine in this solvent are reported in the Supporting Information (Fig. 4S-7S in SI). The addition of iodine or bromine to an acetonitrile solution of **1** was also monitored by UV visible spectroscopy following the absorbance at 226 nm against the time (Fig. 8S in SI) highlighting a faster reaction for bromine.

The reaction of compound **1** with solid iodine was performed in acetonitrile both at room temperature and at 75 °C; invariably providing only compound **2** (see scheme 1).

The well-known formation of small amounts of $[(CH_3CN)_2I]I_3$ was confirmed by UV–visible spectroscopy highlighting a possible active role of the solvent (see section 2S.1 in the SI) [52]. The raw solid of compound **2** was obtained by the concentration of the reaction mixture, and it was crystallized in warm THF and by adding diethyl ether to obtain dark red crystals. Compound **2** crystallizes in the P_{bcn} space group. The structure, shown in Fig. 1, confirmed that carbene remains trans to chlorine atom and the two iodine atoms occupy the remaining positions in the square planar geometry around the metal. The Au1, Cl1 and C1 atoms lye on a 2-fold axis. Only half of the molecule is found in the asymmetric unit. The gold ligand distances are in the range expected for this class of compounds as found from a statistical analysis in the CSD database [44]. The obtained Au-I distances are in agreement with those previously reported in literature [53–54].

The carbene group is rotated by 75.44(3)° respect the coordination plane, due to the interactions between halogen and hydrogen atoms of the neighbouring units. The latter intermolecular contacts contribute to more than 60 % of the Hirshfeld surface area (Figs. 9S and 10S) explaining the rotation of the carbene ligand.

The formation of the square planar product **2** was also highlighted by IR spectroscopy (Fig. 11S and 12S). The FIR spectrum of **2** displays the typical Au-Cl bands at 322 (Au-Cl bands at 330 for the compound **1**) [55]; moreover, it features the disappearance of the band at 248 cm^{-1} and the rising of new bands at 182 cm^{-1}, at 166 cm^{-1} and 153 cm^{-1} assigned to the iodine-Au bonds in trans position to each other. The attribution of these IR bands was made in agreement with the spectroscopic assignments made by Braunstein *et al.* in a series of $LAuX_3$ compounds where X = Cl, Br or I [56]. The ^{1}H NMR spectrum of **2**, shown in Fig. 13S, highlights a shift for the resonance of the imidazole protons from 7.11 ppm of **1** to 7.38 ppm in **2**, while the methyl groups are poorly

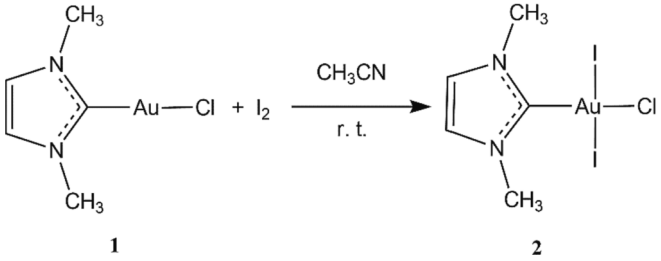

Scheme 1. Synthesis of **2** as $\mathbf{2_{trans}}$ through the reactivity between **1** and I_2.

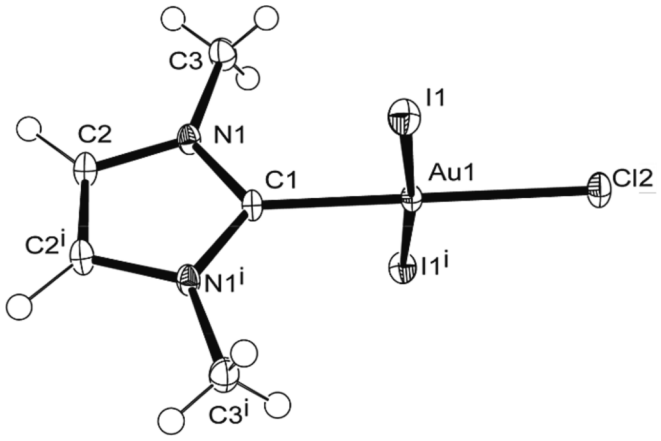

Fig. 1. Molecular structure (ORTEP diagram) of **2** showing the atom labelling scheme. Thermal ellipsoids are shown at a 50 % probability level. Selected bond lengths (Å) and angles (°): Au1-C1 2.003(4); Au1-Cl2 2.3363(11); Au1-I1 2.6124(2); C1-N1 1.345(3); C2-N1 1.384(4); C3-N1 1.466(4); C2-C2′ 1.338 (7); C1-Au1-I1 87.758(5); Cl1-Au1-I1 92.242(5); I1-Au1-I1′ 175.517(10). Symmetry transformations used to generate equivalent atoms: -x + 1,y,-z + 1/2.

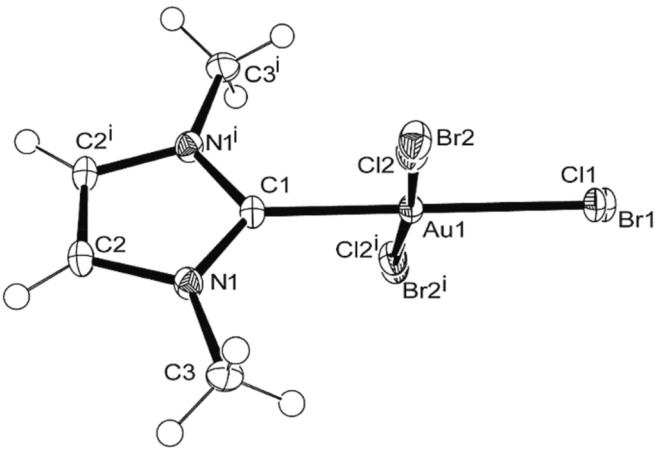

Fig. 2. Molecular structure (ORTEP diagram) of **3** showing the atom labelling scheme. Thermal ellipsoids are shown at a 50 % probability level. Selected bond lengths (Å) and angles (°): Au1-C1 1.993(5); Au1-Cl1 2.319(4); Au1-Br1 2.449 (9); Au1-Cl2 2.289(10); Au1-Br2 4.2288(7); C1-N1 1.347(5); C2-N1 (4) 1.387 (5); C3-N1 1.468(6); C2-C2′ 1.342(9); C1-Au1-Cl2 87(2); C1-Au1-Br2 87.98(7); Cl1-Au1-Br2 92.02(7); Br1-Au1-Br2 92.02(7). The gold halogen distances were restrained to the averaged values (see Experimental section). Symmetry transformations used to generate equivalent atoms: -x + 1, y, -z + 1/2.

sensitive of the coordinative environment at the gold centre displaying only a slight shift from 3.79 ppm of compound **1** to 3.75 ppm in **2** [57]. Traces of other peaks were also detected likely due to the formation of small amount of the cationic bis-carbeneAuI_2 species (Fig. 13S, inset images). Unfortunately, the 1D ^{13}C NMR spectrum was not useful to characterize the compound **2** as the ^{13}C NMR spectra in CD_3CN displays no signal for the NCN carbon, that is instead well visible at 170 ppm in the starting carbene **1** (Fig. 14S). However, the ^{13}C NMR chemical shift was assigned at 134.8 ppm for **2** and at 144.7 ppm for the corresponding bis-carbene resulted to be formed during the long acquisition time in solution, by recording of a ^{1}H ^{13}C HMBC (Hydrogen Multiple Bond Correlation) NMR spectrum on a CD_3CN solution of **2** (Fig. 15S). The reaction of **1** with an excess of iodine was monitored by UV–visible spectroscopy (Figs. 16S and 17S) and only slight electronic re-distributions were observed over the change from linear to a square planar coordination around the gold centre, evidenced by mild shifts of the maxima in the range 210–250 nm.

Differently to iodine, the addition of liquid bromine to 1,3-dimethyl-imidazolyl-2-yl-gold(I)chloride, compound **1**, in acetonitrile solution yields a mixture of cis and trans isomers of the square planar complex **3,** namely $\mathbf{3_{cis}}$ and $\mathbf{3_{trans}}$, respectively (scheme 2).

Red-orange crystals of **3** were grown from an acetonitrile/diethyl ether solution of the raw solid attained from the reaction mixture taken to dryness. While the crystals were isomorphous with **2** (space group P_{bcn}), the disorder in the halogen atom positions is consistent with the presence of both geometrical isomers $\mathbf{3_{cis}}$ and $\mathbf{3_{trans}}$ and their relative content was estimated in 17 % and 83 % respectively, based on the relative occupations for the Cl1/Br1 and Cl2/Br2 atoms. Also, in this case (see Fig. 2) C1, Au1, Cl1 and Br1 atoms lie on the two-fold axis and only half of the molecular structure is reported in the asymmetric unit.

The carbene group is rotated by 70.96(2)° and the overall packing contacts are close to the structure of **2**. Noteworthy, the Au1-C1 and Au1-Cl1 bonds are longer than those observed in the starting compound **1** (Au-C1 1.979 Å in **1** *versus* 2.003 Å in **2** and 1.993 Å in **3**, and Au-Cl1 at 2.288 Å in **1** *versus* 2.3363 Å in **2** and 2.319 Å and 2.289 Å in **3**, see Figs. 1 and 2) [58].

By comparing the IR spectra of $\mathbf{3_{cis/trans}}$ to that of **1,** a richness of bands was observed in the Far IR spectrum recorded for $\mathbf{3_{cis/trans}}$; in fact, it exhibits bands attributable both for the AuCl (328 cm^{-1}) and for the AuBr bonds (246 cm^{-1}, 229 and 185 cm^{-1}). Moreover, the Au-C stretching mode at 465 cm^{-1} is 2 cm^{-1} redshifted compared to the starting compound **1.** An additional band at 455 cm^{-1} was observed possibly due to the C in trans to bromine (the Au-C stretching mode of **2** falls at 464 cm^{-1}) [59]. In solution, compounds $\mathbf{3_{cis/trans}}$ have been studied by ^{1}H NMR, UV–visible spectroscopies and moreover, the reactions of bromine addition to the starting compounds **1** was monitored by IR and UV–visible spectroscopies (Figs. 18S-20S). When the solid of the $\mathbf{3}_{\mathbf{cis/trans}}$ is dissolved in CD_3CN, two patterns of signals (~1: 2 as intensities) are observed in the ^{1}H NMR spectrum, these peaks were attributed to the presence of both cis and trans isomers in solution in different proportion. In fact, the ^{1}H NMR spectrum consists of two doublets for the imidazole C—H protons, at 7.36 and 7.35 ppm, and two singlets at 3.89 and 3.85 ppm for the methyl groups; very small traces of the starting compound **1** were also detected (Figs. 21S and 22S in SI). As concern the ^{13}C NMR, the chemical shifts of compounds $\mathbf{1–3}_{\mathbf{cis/trans}}$ are reported in Table 2 (spectra shown in Fig. 23S). As attained for compound **2**, also the 1D ^{13}C NMR spectrum of $\mathbf{3_{cis/trans}}$ does not display the C1 carbene carbon atoms signals [60–62]; however, the acquisition of the 2D $^{1}H^{13}C$ HMBC spectrum revealed the chemical shifts of **3** with a set

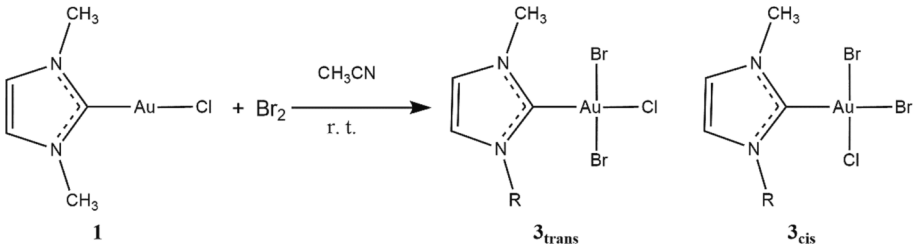

Scheme 2. Synthesis of **3** as $\mathbf{3_{trans}}$ and $\mathbf{3_{cis}}$ through the reactivity between **1** and Br_2.

Table 2
^{13}C NMR chemical shifts in CD_3CN in ppm for compounds **1**-$\mathbf{3_{cis/trans}}$.

Compounds	C1	C2, C2^i	C3, C3^i
1	170.65	122.18	37.57
2	134.8	125.61	37.97
3	133.9 and 136.4 (trans) 136.2 and 138.4 (cis)	125.5 $\mathbf{3_{trans}}$ / 125.4 $\mathbf{3_{cis}}$	37.57 $\mathbf{3_{trans}}$ / 37.40 $\mathbf{3_{cis}}$

of signals at 133.9 and 136 ppm (more intense signals) and at 136.2 and 138.4 ppm (less intense signals) (Fig. 24S).

To verify if the ratio of $\mathbf{3_{cis/trans}}$ isomers in the microcrystalline solid was affected by the temperature, the reaction of bromine and **1** was lead at 0 °C in acetonitrile; the choice of monitoring this reaction depends on the slightly higher solubility of **3** than that of **2**. Differently from what obtained at 20 °C, a precipitate was readily formed (~50 % in mass of yield), which ^1H NMR spectrum recorded at 0 °C highlighted a pattern of signals comparable to those obtained with crystals of $\mathbf{3_{cis/trans}}$ both in intensities and chemical shifts (Fig. 25S and 26S); interestingly, the supernatant to dryness afforded to a pattern of peaks of inverse intensity, likely due to a mixture richer on the $\mathbf{3_{cis}}$ isomer. This latter result has not been replicated by the ^1H NMR spectrum of the 20 °C reaction mixture to dryness (Fig. 27S), highlighting as at lower temperature the formation of $\mathbf{3_{cis}}$ isomer is favored.

3.2. DFT analysis of electronic structures and reactivity

The oxidative addition process, as halogen addition to a linear complex of gold (I), evolves with the formation of a square planar complex with the metal achieving a d^8 count and the bonding generally described within the classic Ligand Field Theory (LF) [63]. In principle, in a gold square planar d^8 transition metal complex, such as $[AuCl_4]^-$ or of NHC-AuX_3 type, four empty metal orbitals, namely 6 s, two 6 ps and one 5d, (d_{x2-y2}), should receive electron donation from four corresponding populated ligands based combinations, assumed to be lower in energy than the metal d orbitals. Thus, according to LF description, the LUMO, or one of the close empty orbitals of a square planar d^8 complex, should have a σ*-antibonding feature with a large contribution from the d_{x2-y2} orbital while the bonding counterpart should be populated and mainly centered on the ligands.

In the last years many exceptions to such an electronic view have been pointed out and the concept of the Inverted Ligand Field [64–71] has been introduced, according to which the gold center never attains the traditionally accepted d^8 count, but it maintains the d^{10} one. This is due to the low-energy gold d orbitals compared to the ligand-based combinations (see scheme 3), thus, in square planar gold complexes the four bonds are better explained in terms of three ligands to metal donations and one metal (from d_{x2-y2}) to ligand interaction. On these bases, the LUMO becomes mainly centered on the ligands rather than on the d metal orbital with the electrons more polarized toward the gold [63]. Scheme 3 summarizes the critical d_{x2-y2} combination in the two

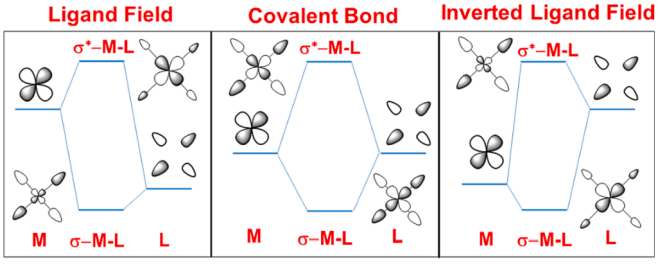

Scheme 3. Sketch of the MO energy levels for a classic Ligand Field approach (left), Inverted Ligand Field (right) and Covalent bonding in the middle.

limiting cases (LF and ILF) as well as the case featuring the metal orbital lying at the same energy of the corresponding ligands based combination, resulting in a pure covalent metal–ligand bonding. The metal contribution to the LUMO becomes a fingerprint of the ILF occurrence with a series of potential situations between the two limiting cases as well as an estimation of the covalent contribution of the M−L bond. The ILF shows more electron richer metal centers compared to the crude description of the electronic distribution given by the common oxidation state rules. Such an electronic distribution has been already suggested for some gold square planar complexes such as $[AuCl_4]^-$ [64] as well as in bi-metallic Au/Fe clusters [65].

n order to verify the ILF occurrence or not in the present square planar complexes, a detailed theoretical investigation on the electronic structure of the isolated square planar complexes $\mathbf{2_{trans}}$, $\mathbf{3_{cis}}$ and $\mathbf{3_{trans}}$ has been carried out. As aforementioned, in the ILF description the LUMO becomes centered on the ligands rather than the metal orbital and *vice versa* for the bonding counterpart (see scheme 3). Fig. 3 reports the plot of the LUMO for $\mathbf{2_{trans}}$, $\mathbf{3_{trans}}$ and $\mathbf{3_{cis}}$ products highlighting the σ* character together with the metal contribution (from the d_{x2-y2} orbital).

The electronic analysis pointed out the occupancy of all the d metal orbitals (see Table S1), the LUMO bonding counterparts are mainly localized on the populated d_{x2-y2} metal orbital. The gold center in these square planar complexes never attains the expected d^8 electronic count but maintains the starting d^{10} one with a σ back donation into an empty ligands' combination. This point is supported by the Natural Bonding Analysis [72] revealing a d orbitals occupation between 9.4 and 9.5 electrons. Such obtained alternative electronic structure does not fit with the generally accepted classification as oxidative addition of the halogen addition to linear gold(I) complexes. Similar results have been obtained also through the calculations on the optimized structures considering the ZORA relativistic corrections for the gold and iodine centers.

Among all the potential reaction pathways taken herein in consideration, DFT analysis revealed that the most probable one was the stepwise addition of halogen centers to the linear gold(I) complex starting with the introduction of a halonium. Thus, *T*-shape cationic intermediates have been detected featuring a carbene, a chloride and the newly entered halonium ligand together with a released halide moiety. The electronic structure of the cationic *T*-shape intermediates invariably revealed a d^{10} configuration of the gold center with the presence of an empty molecular orbital (namely the LUMO shown in Fig. 28S) able to interact with the released halide anion, providing the square planar products. This is another confirmation of the unrealistic classification of the halogen addition as oxidative addition. A similar behavior has been pointed out by some of us for the "oxidative addition" of a Se-Cl linkage over a square planar Pt (II) complex reaching the final octahedral arrangement. Also in that case, the metal never attains the expected classic assigned d^6 configuration since the Se-Cl activation occurs through a square-pyramidal cationic species with an empty orbital on the platinum center [73].

Another interesting feature of such a reactivity highlighted by the DFT analysis was the potential isomerization of the *T*-shape intermediates. As shown in Scheme 4, the cationic *T*-shape tri-coordinate intermediate features two different kinds of coordination sites: two "longitudinal" positions (called LON in scheme 4) and one in between the latter, called "transversal" (called TR in scheme 4).

In the case of the iodine addition, two other different isomers are potentially available for the cation $\mathbf{4_a^+}$, alternatively featuring the localization of the three ligands (carbene, iodine and chlorine) in the longitudinal sites.

Thus, next to the obtained cationic *T*-shaped $\mathbf{4_a}^+$ an isomer, namely $\mathbf{4_b}^+$ shown in Fig. 4 formally obtaining by the 90° in-plane rotation of chlorine, was found to be more stable in free energy by −0.9 kcal mol^{-1}. In both cases, the analysis of the electronic structure suggests a d^{10} metal configuration, as confirmed by the contribution of the ligands to the LUMO (70 % mainly from carbene and iodine *vs.* 30 % from gold). An

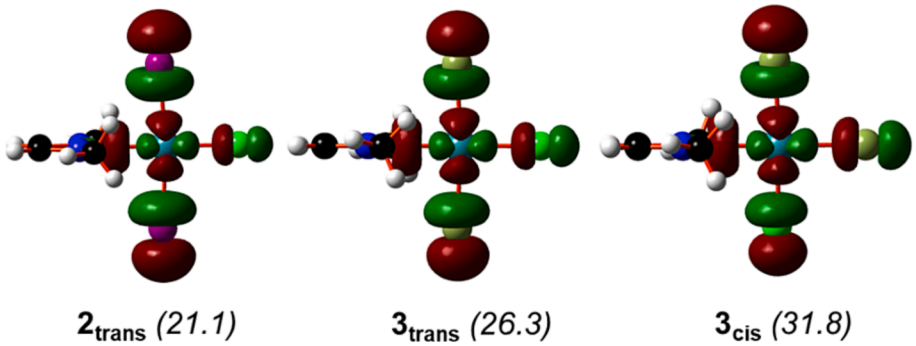

Fig. 3. Plot of the Lowest Unoccupied Molecular Orbital in the three-square planar crystal structures: $\mathbf{2}_{trans}$, $\mathbf{3}_{trans}$ and $\mathbf{3}_{cis}$. The % contribution from the d gold orbital is reported in brackets.

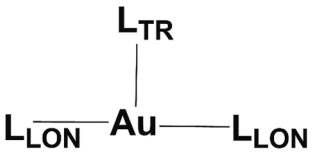

Scheme 4. Representation of the coordination sites around the Au center in a *T*-shape intermediate as $\mathbf{4}_{a}{}^{+}$.

electronic depletion on the ligands, especially from the carbene and the iodine ones, is expected respect to the classical d^8 description. The NBO analysis [72] revealed an electronic population of 9.4 electrons for the metal d orbitals in both the *T*-shape intermediates equal to that found in the square planar complexes, once again suggesting the improbable assignment of a d^8 configuration. The optimization starting from the third potential *T*-shape isomer, called $\mathbf{4}_{c}{}^{+}$ formally obtained by a 90° in-plane rotation of iodine from $\mathbf{4}_{b}^{+}$ shown in Fig. 4, converged in any case to $\mathbf{4}_{b}^{+}$. This result agrees with those obtained for *T*-shape Pt(II) complexes, for which detailed computational analysis have pointed out the improbable localization of the most electronegative atom in the transversal position [74–76].

In principle, both the two isomers are plausible in view of the closeness of the electronegativity values of carbon and iodine, computationally confirmed by free energy difference lower than 1 kcal mol^{-1}). In any case, the final square planar complexes obtained by the reaction between the two isomers $\mathbf{4}_{a}^{+}$ and $\mathbf{4}_{b}^{+}$ with the released iodide featured an inversion in the free energy stability, with the product from $\mathbf{4}_{a}^{+}$(featuring the two iodine in trans configuration) more stable by *ca.* 6.3 kcal mol^{-1} than the other one (with the two iodine in cis configuration).

Alternatively, the addition of Br_2 to the linear complex 1,3-dimethylimidazolyl-2yl-gold(I) chloride, **1**, has provided two isomeric square planar complexes $\mathbf{3}_{cis}$ and $\mathbf{3}_{trans}$ in 17 % *vs.* 83 % proportion. The *T*-shape intermediate $\mathbf{5}_{b}^{+}$, shown in Fig. 5 featuring the chloride and the bromide trans each other, is more stable than the corresponding isomer $\mathbf{5}_{a}^{+}$, by −6.5 kcal mol^{-1}, six times larger than the energy difference between the two isomers in the case of the iodine. As in the case of the iodine addition, also for bromine the square planar final complex featuring the two introduced bromine in trans configuration has been estimated to be more stable by *ca.* 2 kcal mol^{-1}.

In view of the very low free energy differences between the calculated isomers, the processes can be easily perturbed by secondary interactions affecting the final ratio of the geometrical isomers in the solid state. In any case, as a general guideline, the DFT analysis revealed that the isomer with the most electronegative atom in the axial positions is the most stable. Thus, the addition of a more electronegative element such as bromine in place of iodine should result in a bigger free energy difference between the two isomers. Scheme 5 highlights the free energy stability of the cis/trans *T*-shape cationic isomers from the insertion of different halogen atom from iodine up to the chlorine, the latter one only computationally addressed as well as the addition of fluorine. In the limiting case of the fluorine insertion, the only possible optimized isomer is the trans one, once again suggesting the improbable localization of the most electronegative atom in the transversal position.

4. Conclusions

The reactivity between halogens and linear Au(I) complexes, leading to the formation of square planar compounds, is traditionally classified

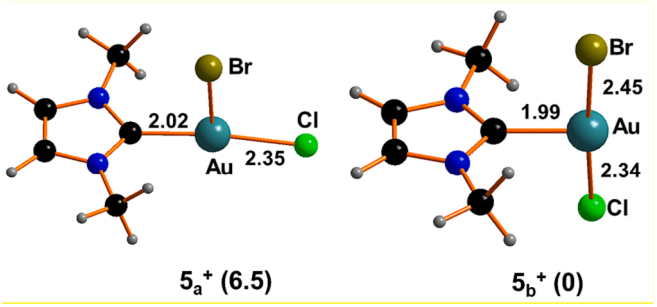

Fig. 5. Optimized structure of cationic *T*-shape isomers: $\mathbf{5}_{a}{}^{+}$ and $\mathbf{5}_{b}{}^{+}$. The relative free energies in kcal mol^{-1} are provided in brackets.

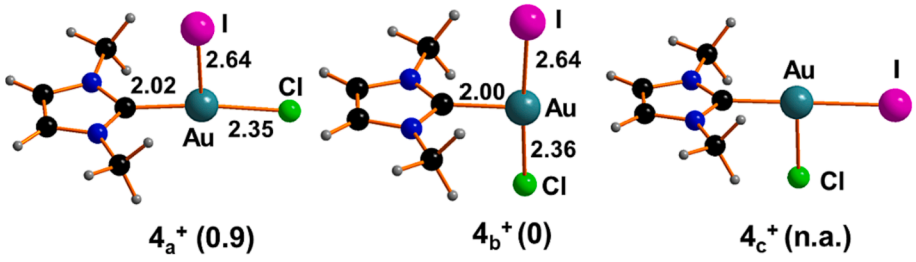

Fig. 4. Potential three structural isomers of cationic *T*-shape $\mathbf{4}^{+}$. The relative free energy stability in kcal mol^{-1} is given in round brackets.

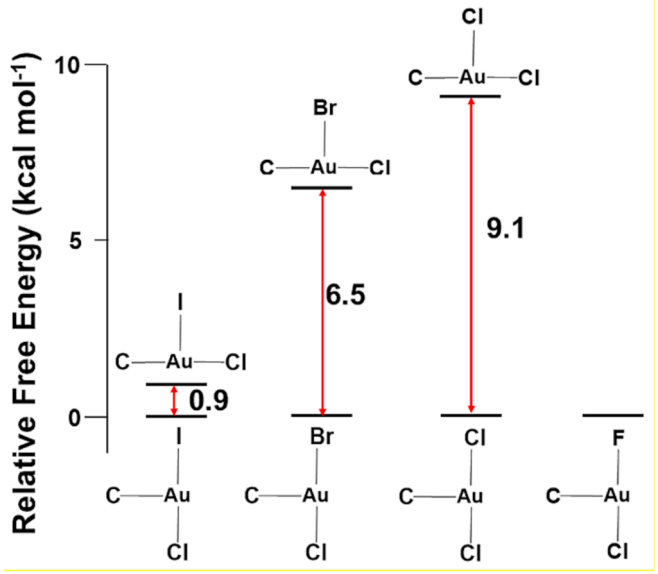

Scheme 5. Relative Free Energy (kcal mol^{-1}) for the different cationic *T*-shape isomers obtained through the addition of one iodine, bromine, chlorine and fluorine atom. The hypothetical addition of a fluorine atom invariably provides the isomer with fluorine and chlorine in trans arrangement, while for iodine, bromine and chlorine addition, a and b type isomers were found.

as an oxidative addition process causing the increase of the oxidation number of two units. The addition reactions of I_2 and Br_2 to linear 1,3-dimethylimazolyl-2yl-gold chloride compound **1** were monitored at room temperature, at 0 °C and 75 °C in order to clarify the relationship between the obtained products and all the electronic factors and the possible isomerization processes, ruling this kind of reactivity. The results showed that the addition of iodine leads to the exclusive isolation of the *trans*-square planar isomer, while the addition of bromine provides both cis/trans isomers in a ratio of 17 and 83 % respectively, as evidenced by single crystal X-ray structural characterizations. The bonding pattern has been explained in the framework of the Inverted Ligand Field, that suggests an electronic d^{10} count for gold and a donation of $d_{x2\text{-}y2}$ metal orbital electrons into an empty ligand combination, as confirmed by the small contribution of the d gold orbital to the LUMO. Accordingly, DFT calculations highlighted a covalent gold-ligand bonding with a metal center electronically richer than in the classic Ligand Field description, confirming the ILF occurrence. The manuscript completely revised the concept of the oxidative addition process to gold(I) linear complexes with the stepwise insertion of halogen atoms consisting on a first step with the introduction of the halonium cations, and the formation of *T*-shape cationic intermediates. Furthermore, the DFT analysis highlighted the possible occurrence of isomerization processes for the intermediates with those featuring the two halogen centers in trans position more stable than those with the cis arrangement. In any case, the calculated free energy differences between isomers are very low and the final ratio of the isomers may be affected also by other processes. This manuscript provides some guidelines for better understanding the reactivity of the gold(I) complexes and for the design of new efficient synthetic pathway.

CRediT authorship contribution statement

Rossana Galassi: Conceptualization, Writing – original draft, Writing – review & editing, Supervision. **Nicola Sargentoni:** Methodology, Investigation, Data curation. **Lorenzo Luciani:** Methodology, Investigation. **Gabriele Manca:** Conceptualization, Writing – review & editing, Investigation. **Andrea Ienco:** Conceptualization, Writing – review & editing, Investigation.

Declaration of Competing Interest

The authors declare that they have no known competing financial interests or personal relationships that could have appeared to influence the work reported in this paper.

Data availability

Data will be made available on request.

Acknowledgments

RG is grateful to the University of Camerino for the financial support through the Fondi di Ateneo per la Ricerca, FAR.

Appendix A. Supplementary data

CCDC 2240409 and 2240407 contain the supplementary crystallographic data for this paper. Supplementary data to this article can be found online at https://doi.org/10.1016/j.ica.2023.121810.

References

[1] J. Halpern, Oxidative-Addition Reactions of Transition Metal Complexes, Acc. Chem. Res. 3 (1970) 386–392, https://doi.org/10.1021/ar50035a004.
[2] E. Boros, P.J. Dyson, G. Gasser, Classification of Metal-Based Drugs According to Their Mechanisms of Action, Chem 6 (2020) 41–60, https://doi.org/10.1016/j.chempr.2019.10.013.
[3] L. Souillart, N. Cramer, Catalytic C-C Bond Activations via Oxidative Addition to Transition Metals, Chem. Rev. 115 (2015) 9410–9464, https://doi.org/10.1021/acs.chemrev.5b00138.
[4] T. Sperger, I.A. Sanhueza, I. Kalvet, F. Schoenebeck, Computational Studies of Synthetically Relevant Homogeneous Organometallic Catalysis Involving Ni, Pd, Ir, and Rh: An Overview of Commonly Employed DFT Methods and Mechanistic Insights, Chem. Rev. 115 (2015) 9532–9586, https://doi.org/10.1021/acs.chemrev.5b00163.
[5] J.A. Labinger, Tutorial on Oxidative Addition, Organometallics 34 (2015) 4784–4795, https://doi.org/10.1021/acs.organomet.5b00565.
[6] J.B. Diccianni, J. Katigbak, C. Huand, T. Diao, Mechanistic Characterization of (Xantphos)Ni(I)-Mediated Alkyl Bromide Activation: Oxidative Addition, Electron Transfer, or Halogen-Atom Abstraction, J. Am. Chem. Soc. 141 (2019) 1788–1796, https://doi.org/10.1021/jacs.8b13499.
[7] D.P. Hickey, C. Sandford, Z. Rhodes, T. Gensch, L.R. Fries, M.S. Sigman, S. D. Minteer, Investigating the Role of Ligand Electronics on Stabilizing Electrocatalytically Relevant Low-Valent Co(I) Intermediates, J. Am. Chem. Soc. 141 (2019) 1382–1392, https://doi.org/10.1021/jacs.8b12634.
[8] H. Kawai, W.J. Wolf, A.G. Dipasquale, M.S. Winston, F.D. Toste, Phosphonium Formation by Facile Carbon-Phosphorus Reductive Elimination from Gold(III), J. Am. Chem. Soc. 138 (2016) 587–593, https://doi.org/10.1021/jacs.5b10720.
[9] J.F. Hartwig, Electronic Effects on Reductive Elimination to Form Carbon-Carbon and Carbon-Heteroatom Bonds from Palladium(Ll) Complexes, Inorg. Chem. 46 (2007) 1936–1947, https://doi.org/10.1021/ic061926w.
[10] F. Vizza, Giano Lacinio Alchimista Francescano del Cinquecento Laruffa Editore 2014 ISBN 978-88-7221-748-1.
[11] L.J. Beckham, W.A. Fessler, M.A. Kise, Nitrosyl Chloride, Chem. Rev. 48 (1951) 319–396, https://doi.org/10.1021/cr60151a001.
[12] M.J. Harper, C.J. Arthur, J. Crosby, E.J. Emmett, R.L. Falconer, A.J. Fensham-Smith, P.J. Gates, T. Leman, J.E. McGrady, J.F. Bower, C.A. Russell, Oxidative Addition, Transmetalation, and Reductive Elimination at a 2,2′-Bipyridyl-Ligated Gold Center, J. Am. Chem. Soc. 140 (2018) 4440–4445, https://doi.org/10.1021/jacs.8b01411.
[13] M. Livendahl, C. Goehry, F. Maseras, A.M. Echavarren, Rationale for the Sluggish Oxidative Addition of Aryl Halides to Au(I), Chem. Commun. 50 (2014) 1533–1536, https://doi.org/10.1039/C3CC48914K.
[14] J.H. Teles, Oxidative Addition to Gold(I): A New Avenue in Homogeneous Catalysis with Au, Angew. Chemie Int. Ed. 54 (2015) 5556–5558, https://doi.org/10.1002/anie.201501966.
[15] Y. Yang, L. Eberle, F.F. Mulks, J.F. Wunsch, M. Zimmer, F. Rominger, M. Rudolph, A.S.K. Hashmi, Trans Influence of Ligands on the Oxidation of Gold(I) Complexes, J. Am. Chem. Soc. 141 (2019) 17414–17420, https://doi.org/10.1021/jacs.9b09363.
[16] D. Schneider, A. Schier, H. Schmidbaur, Governing the Oxidative Addition of Iodine to Gold(I) Complexes by Ligand Tuning, Dalton Trans. 13 (2004) 1995–2005, https://doi.org/10.1039/B403005B.
[17] M. Baron, C. Tubaro, M. Basato, A. Biffis, M.M. Natile, C. Graiff, Dinuclear N-Heterocyclic Dicarbene Gold Complexes in I-III and III–III Oxidation States: Synthesis and Structural Analysis, Organometallics 30 (2011) 4607–4615, https://doi.org/10.1021/om2004145.

[18] M. Baron, C. Tubaro, M. Basato, A.A. Isse, A. Gennaro, L. Cavallo, C. Graiff, A. Dolmella, L. Falivene, L. Caporaso, Insights into the Halogen Oxidative Addition Reaction to Dinuclear Gold(I) Di(nhc) Complexes, Chem.–a Eur. J. 22 (2016) 10211–10224, https://doi.org/10.1002/chem.201600654.

[19] C.Y. Wu, T. Horibe, C.B. Jacobsen, F.D. Toste, Stable Gold(III) Catalysts by Oxidative Addition of a Carbon-Carbon Bond, Nature 517 (2015) 449–454, https://doi.org/10.1038/nature14104.

[20] S. Komiya, T.A. Albright, R. Hoffmann, J.K. Kochi, Reductive Elimination and Isomerization of Organogold Complexes. Theoretical Studies of Trialkylgold Species as Reactive Intermediates. Stability of Organogold(III) Complexes. Isolation and Crystal Structure of Dimethylgold Trifluoromethanesulfonate, J. Am. Chem. Soc. 98 (1976) 7255–7265, https://doi.org/10.1021/ja00439a024.

[21] M.S. Winston, W.J. Wolf, F.D. Toste, Halide-Dependent Mechanisms of Reductive Elimination from Gold(III), J. Am. Chem. Soc. 137 (2015) 7921–7928, https://doi.org/10.1021/jacs.5b04613.

[22] D. Schneider, O. Schuster, H. Schmidbaur, Attempted Oxidative Addition of Halogens to (Isocyanide)Gold(I) Complexes, Organometallics 24 (2005) 3547–3551, https://doi.org/10.1021/om0502739.

[23] P. De Frémont, R. Singh, E.D. Stevens, J.L. Petersen, S.P. Nolan, Synthesis, Characterization and Reactivity of N-Heterocyclic Carbene Gold(III) Complexes, Organometallics 26 (2007) 1376–1385, https://doi.org/10.1021/om060887t.

[24] S. Vanicek, J. Beerhues, T. Bens, V. Levchenko, K. Wurst, B. Bildstein, M. Tilset, B. Sarkar, Oxidative Access via Aqua Regia to an Electrophilic, Mesoionic Dicobaltoceniumyltriazolylidene Gold(III) Catalyst, Organometallics 38 (2019) 4383–4386, https://doi.org/10.1021/acs.organomet.9b00616.

[25] M. Kriechbaum, D. Otte, M. List, U. Monkowius, Facile Oxidation of NHC-Au(I) to NHC-Au(III) Complexes by CsBr 3, Dalton Trans. 43 (2014) 8781–8791, https://doi.org/10.1039/C4DT00695J.

[26] A. Portugués, D. Bautista, J. Gil-Rubio, Dinuclear Au(I), Au(II) and Au(III) Complexes with (CF2)n Chains: Insights into The Role of Aurophilic Interactions in the Au(I) Oxidation, Chem. – A Eur. J. 27 (2021) 15815–15822, https://doi.org/10.1002/chem.202103153.

[27] A. Portugués, M.A. Martínez-Nortes, D. Bautista, P. González-Herrero, J. Gil-Rubio, Reductive Elimination Reactions in Gold(III) Complexes Leading to C(sp3)-X (X = C, N, P, O, Halogen) Bond Formation: Inner-Sphere vs SN2 Pathways, Inorg. Chem. 62 (2022) 1708–1718, https://doi.org/10.1021/acs.inorgchem.2c04166.

[28] G. Yang, R.G. Raptis, Oxidation of Gold(I) Pyrazolates by Aqua Regia. X-Ray Crystal Structures of the First Examples of Trinuclear AuIII3 and AuIAuIII2 Pyrazolato Complexes, J. Chem. Soc. Dalton Trans. 268 (2002) 3936–3938, https://doi.org/10.1039/B207600D.

[29] K. Klauke, I. Gruber, T.O. Knedel, L. Schmolke, J. Barthel, H. Breitzke, G. Buntkowsky, C. Janiak, Silver, Gold, Palladium, and Platinum N-Heterocyclic Carbene Complexes Containing a Selenoether-Functionalized Imidazol-2-Ylidene Moiety, Organometallics 37 (2018) 298–308, https://doi.org/10.1021/acs.organomet.7b00678.

[30] S. Orbisaglia, B. Jacques, P. Braunstein, D. Hueber, P. Pale, A. Blanc, P. De Frémont, Synthesis, Characterization, and Catalytic Activity of Cationic NHC Gold (III) Pyridine Complexes, Organometallics 32 (2013) 4153–4164, https://doi.org/10.1021/om400338k.

[31] C. Hirtenlehner, C. Krims, J. Hölbling, M. List, M. Zabel, M. Fleck, R.J.F. Berger, W. Schoefberger, U. Monkowius, Syntheses, Crystal Structures, Reactivity, and Photochemistry of Gold(III) Bromides Bearing N-Heterocyclic Carbenes, Dalton Trans. 40 (2011) 9899–9910, https://doi.org/10.1039/C1DT11175B.

[32] C. Topf, C. Hirtenlehner, M. Zabel, M. List, M. Fleck, U. Monkowius, Synthesis and Characterization of Silver(I), Gold(I), and Gold(III) Complexes Bearing Amino-Functionalized N-Heterocyclic Carbenes, Organometallics 30 (2011) 2755–2764, https://doi.org/10.1021/om2000713.

[33] S. Attar, J.H. Nelson, W.H. Bearden, N.W. Alcock, L. Solujic', E.B. Milosavljevic', Phosphole Complexes of Gold(III) Halides: Synthesis, Structure, Electrochemistry and Ligand Redistribution Reactions, Polyhedron 10 (16) (1991) 1939–1949.

[34] D. Lanari, M.C. Marcotullio, A. Neri, A Design of Experiment Approach for Ionic Liquid-Based Extraction of Toxic Components-Minimized Essential Oil from Myristica Fragrans Houtt, Fruits, Molecules 23 (2018) 2817, https://doi.org/10.3390/molecules23112817.

[35] R. Visbal, A. Laguna, M.C. Gimeno, Simple and Efficient Synthesis of [MCI(NHC)] (M = Au, Ag) Complexes, Chem. Commun. 49 (50) (2013) 5642.

[36] E.A. Martynova, N.V. Tzouras, G. Pisanò, C.S.J. Cazin, S.P. Nolan, The "weak base route" leading to transition metal–N-heterocyclic carbene complexes, Chem. Commun. 57 (2021) 3836–3856, https://doi.org/10.1039/D0CC08149C.

[37] APEX2 Software | Bruker https://www.bruker.com/en/products-and solutions/diffractometers-and-scattering-systems/single-crystal-x-ray-diffractometers/sc-xrd-software/apex.html (accessed Jun 28, 2021).

[38] Bruker Bruker SAINT; Bruker AXS Inc.: Madison, Wisconsin, USA, 2012.

[39] L. Krause, R. Herbst-Irmer, G.M. Sheldrick, D. Stalke, Comparison of silver and molybdenum microfocus X-ray sources for single-crystal structure determination, J. Appl. Cryst. 48 (2015) 3–10, https://doi.org/10.1107/S1600576714022985.

[40] M.C. Burla, R. Caliandro, M. Camalli, B. Carrozzini, G.L. Cascarano, L. Da Caro, C. Giacovazzo, G. Polidori, R. Spagna, An improved tool for crystal structure determination and refinement, J. Appl. Cryst. 38 (2005) 381–388, https://doi.org/10.1107/S002188980403225X.

[41] G.M. Sheldrick, Crystal structure refinement with SHELXL, Acta Crystallogr., Sect. C: Struct. Chem. C71 (2015) 3–8, https://doi.org/10.1107/S2053229614024218.

[42] L. Branzi, M. Baron, L. Armelao, M. Rancan, P. Sgarbossa, C. Graiff, A. Pöthig, A. Biffis, Coordination Chemistry of Gold with N-Phosphine Oxide-Substituted Imidazolylidenes (POxIms), New J. Chem. 43 (2019) 17275–17283, https://doi.org/10.1039/C9NJ04911H.

[43] S. Parkin, J. Cunningham, B. Rawls, J.E. Bender, R.J. Staples, S.M. Biros, A mixed phosphine sulfide/selenide structure as an instructional example for how to evaluate the quality of a model, Acta Crystallogr, Sect. e. 79 (4) (2023) 246–253.

[44] C.R. Groom, I.J. Bruno, M.P. Lightfoot, S.C. Ward, The Cambridge Structural, Database 72 (2016) 171–179.

[45] P. R. Spackman, M. J. Turner, J. J. McKinnon, S. K. Wolff, D. J. Grimwood, D. Jayatilaka, M. A. Spackman, CrystalExplorer: A Program for Hirshfeld Surface Analysis, Visualization and Quantitative Analysis of Molecular Crystals 54 (2021) 1006–1011.

[46] S. Grimme, Semiempirical Hybrid Density Functional with Perturbative Second-Order Correlation, J. Chem. Phys. 124 (2006) 6158, https://doi.org/10.1063/1.2148954.

[47] M. J. Frisch, G. W. Trucks, H. B. Schlegel, G. E. Scuseria, M.A. Robb, J. R. Cheeseman, G. Scalmani, V. Barone, G. A. Petersson, H. Nakatsuji, X. Li, M. Caricato, A. V. Marenich, J. Bloino, B. G. Janesko, R. Gomperts, B. Mennucci, H. P. Hratchian, J. V. Ortiz, A. F. Izmaylov, J. L. Sonnenberg, D. Williams-Young, F. Ding, F. Lipparini, F. Egidi, J. Goings, B. Peng, A. Petrone, T. Henderson, D. Ranasinghe, V. G. Zakrzewski, J. Gao, N. Rega, G. Zheng, W. Liang, M. Hada, M. Ehara, K. Toyota, R. Fukuda, J. Hasegawa, M. Ishida, T. Nakajima, Y. Honda, O. Kitao, H. Nakai, T. Vreven, K. Throssell, J. A. Jr. Montgomery, J. E. Peralta, F. Ogliaro, M. J. Bearpark, J. J. Heyd, E. N. Brothers, K. N. Kudin, V. N. Staroverov, T. A. Keith, R. Kobayashi, J. Normand, K. Raghavachari, A. P. Rendell, J. C. Burant, S. S. Iyengar, J. Tomasi, M. Cossi, J. M.; Millam, M. Klene, C. Adamo, R. Cammi, J. W. Ochterski,R. L. Martin, K. Morokuma, O. Farkas, J. B. Foresman and D. J. Fox, Gaussian 16, revision C.01; Gaussian, Inc.: Wallingford, CT, 2016.

[48] C. Adamo, V. Barone, Quantum Calculation of Molecular Energies and Energy Gradients in Solution by a Conductor Solvent Model, J. Chem. Phys. 110 (1999) 6158–6169, https://doi.org/10.1021/jp9716997.

[49] M. Dolg, H. Stoll, H. Preuss, R.M. Pitzer, Relativistic and correlation effects for element 105 (hahnium, Ha): a comparative study of M and MO (M = Nb, Ta, Ha) using energy-adjusted ab initio pseudopotentials, J. Phys. Chem. 97 (22) (1993) 5852–5859.

[50] A. Schäfer, C. Huber, R. Ahlrichs, Fully Optimized Contracted Gaussian Basis Sets of Triple Zeta Valence Quality for Atoms Li to Kr, J. Chem. Phys. 100 (8) (1994) 5829–5835.

[51] F. Neese, Software Update: The ORCA Program System—Version 5.0. Wiley Interdiscip, Rev. Comput. Mol. Sci. 12 (2022) e1606.

[52] Y. Nakao, K. Sone, Reversible Dissolution/Deposition of Gold in Iodine–Iodide–Acetonitrile Systems, Chem. Commun. 897 (1996) 897–898, https://doi.org/10.1039/CC9960000897.

[53] H.V. Huynh, S. Guo, W. Wu, Detailed Structural, Spectroscopic, and Electrochemical Trends of Halido Mono- and Bis(NHC) Complexes of Au(I) and Au (III), Organometallics 32 (2013) 4591–4600, https://doi.org/10.1021/om400563e.

[54] J. M. Holthoff, E. Engelage, A. B. Kowsari, S. M. Huber, R. Weiss Noble Metal Corrosion: Halogen Bonded Iodocarbenium Iodides Dissolve Elemental Gold—Direct Access to Gold–Carbene Complexes Chem.- E. J. 25 (2019) 7480-7484. doi: 10.1002/chem.201901583.

[55] A.E. O'Connor, N. Mirzadeh, S.K. Bhargava, T.L. Easun, M. Schröder, A.J. Blake, Aurophilicity under pressure: a combined crystallographic and *in situ* spectroscopic study, Chem. Commun. 52 (2016) 6769–6772, https://doi.org/10.1039/C6CC00923A.

[56] P. Braunstein, R.J.H. Clark, W. Ramsay, R. Forster, C. Lngold, The Preparation, Properties, and Vibrational Spectra of Complexes Containing the AuCl2–, AuBr 2–, and AuI2– Ions, J. Chem. Soc. Dalton Trans. (1973) 1845–1848, https://doi.org/10.1039/DT9730001845.

[57] F. Guarra, A. Terenzi, C. Pirker, R. Passannante, D. Baier, E. Zangrando, V. Gómez-Vallejo, T. Biver, C. Gabbiani, W. Berger, J. Llop, L. Salassa, 124I Radiolabeling of a Au III -NHC Complex for In Vivo Biodistribution Studies, Angew. Chem. 132 (2020) 17278–17284, https://doi.org/10.1002/anie.202008046.

[58] M.J. Harrison, C.S.V. Wang, T.Y.R. Tsai, C. Shih-Hua, A.H.H. Chang, I.J.B. Lin, Gold(I) N-Heterocyclic Carbene and Carbazolate Complexes, Organometallics 24 (2005) 486–493, https://doi.org/10.1021/om049221u.

[59] E. Husson, N. Quy Dao, D.K. Breitinger, Vibrational Spectra and Normal Coordinate Analyses of the Gold Halides AuX (X = Cl, Br and I), Spectrochim. Acta Part A Mol. Spectrosc. 37 (1981) 1087–1092, https://doi.org/10.1016/0584-8539(81)80154-7.

[60] D. Tapu, D.A. Dixon, C. Roe, ^{13}C NMR Spectroscopy of "Arduengo-Type" Carbenes and Their Derivatives, Chem. Rev. 109 (2009) 3385–3407, https://doi.org/10.1021/cr800521g.

[61] H.T. Liu, X.G. Xiong, P. Diem Dau, Y.L. Wang, D.L. Huang, J. Li, L.S. Wang, Probing the Nature of Gold-Carbon Bonding in Gold-Alkynyl Complexes, Nat. Commun. 4 (2013) 1–7, https://doi.org/10.1038/ncomms3223.

[62] S. Gaillard, A.M.Z. Slawin, A.T. Bonura, E.D. Stevens, S.P. Nolan, Synthetic and Structural Studies of [AuCl3(NHC)] Complexes, Organometallics 29 (2010) 394–402, https://doi.org/10.1021/om900814e.

[63] R. Hoffmann, S. Alvarez, C. Mealli, A. Falceto, T.J. Cahill, T. Zeng, G. Manca, From Widely Accepted Concepts in Coordination Chemistry to Inverted Ligand Fields, Chem. Rev. 116 (14) (2016) 8173–8192.

[64] R. Galassi, L. Luciani, C. Graiff, G. Manca, A Reinterpretation of the Imidazolate Au (I) Cyclic Trinuclear Compounds Reactivity with Iodine and Methyl Iodide with the Perspective of the Inverted Ligand Field Theory, Inorg. Chem. 61 (2022) 3527–3539, https://doi.org/10.1021/acs.inorgchem.1c03492.

[65] G. Manca, F. Fabrizi de Biani, M. Corsini, C. Cesari, C. Femoni, M.C. Iapalucci, S. Zacchini, A. Ienco, Inverted Ligand Field in a Pentanuclear Bow Tie Au/Fe

Carbonyl Cluster, Inorg. Chem. 61 (2022) 3484–3492, https://doi.org/10.1021/acs.inorgchem.1c03386.
[66] D. Joven-Sancho, M. Baya, A. Martín, J. Orduna, B. Menjón, Five-Coordinate Compound with Inverted Ligand Field: An Unprecedented Geometry for Silver(III), Angew. Chemie Int. Ed. 60 (2021) 26545–26549, https://doi.org/10.1002/anie.202112449.
[67] A. Pérez-Bitrián, M. Baya, J.M. Casas, A. Martín, B. Menjón, Hydrogen Bonding to Metals as a Probe for an Inverted Ligand Field, Dalton Trans. 50 (2021) 5465–5472, https://doi.org/10.1039/D1DT00597A.
[68] E.D. Litle, F.P. Gabbaï, A Cationic Gold-Fluorenyl Complex with a Dative Au → C+ Bond: Synthesis, Structure, and Carbophilic Reactivity, Chem. Commun. 59 (2023) 603–606, https://doi.org/10.1039/D2CC05436A.
[69] E.A. Trifonova, I.F. Leach, W.B. de Haas, R.W.A. Havenith, M. Tromp, J.E.M. Klein, Spectroscopic Manifestations and Implications for Catalysis of Quasi-d10 Configurations in Formal Gold(III) Complexes, Angew. Chemie 135 (2023) e202215523.
[70] I.M. Dimucci, J.T. Lukens, S. Chatterjee, K.M. Carsch, C.J. Titus, S.J. Lee, D. Nordlund, T.A. Betley, S.N. MacMillan, K.M. Lancaster, The Myth of d8 Copper (III), J. Am. Chem. Soc. 141 (2019) 18508–18520, https://doi.org/10.1021/jacs.9b09016.
[71] R.C. Walroth, J.T. Lukens, S.N. MacMillan, K.D. Finkelstein, K.M. Lancaster, Spectroscopic Evidence for a 3d10 Ground State Electronic Configuration and Ligand Field Inversion in [Cu(CF3)4]-, J. Am. Chem. Soc. 138 (2016) 1922–1931, https://doi.org/10.1021/jacs.5b10819.
[72] F. Weinhold, Natural bond orbital analysis: A critical overview of relationships to alternative bonding perspectives, J. Comput. Chem. 33 (2012) 2363–2379, https://doi.org/10.1002/jcc.23060.
[73] A. Ienco, F. Ruffo, G. Manca, The Role of Inverted Ligand Field in the Electronic Structure and Reactivity of Octahedral Formal Platinum (IV), Complexes, Chem. Eur. J. (2023), e202301669, https://doi.org/10.1002/chem.202301669.
[74] D. Sturmayr, U. Schubert, Ab-initio Calculations of T-shaped Phosphine-Platinum (II) Complexes, Monatshefte fur Chemie 134 (2003) 791–795, https://doi.org/10.1007/s00706-002-0568-6.
[75] M.A. Ortuño, S. Conejero, A. Lledós, True and masked three-coordinate T-shaped platinum(II) intermediates Beilstein, J. Org. Chem. 9 (2013) 1352–1382, https://doi.org/10.3762/bjoc.9.153.
[76] A. Ienco, D.M. Proserpio, R. Hoffmann, Main Group Element Nets to a T, Inorg. Chem. 43 (2004) 2526–2540, https://doi.org/10.1021/ic0353211.